VI. Conclusion

The planar L-slot antenna fed with a W-shaped stub can be modified to have a bent ground plane. The ground plane modification does affect impedance matching but this can be rectified easily by readjusting the stub length. However, the comparison of radiation patterns is complicated. The effect on UWB radiation performance and pattern stability over this ultrawide bandwidth is not obvious from visual inspection of the radiation patterns. Therefore, it is essential to use an appropriate figure of merit for comparing the radiation pattern stability. Our investigation indicates that structural modifications may improve or degrade the pattern stability, depending on the range of directions and polarizations considered. A more realistic assessment of UWB radiation performance can be obtained by restricting the PSF calculation to the directions with high radiated energy. Both the planar and the modified MLSA have very good UWB performance in those directions.

The two antennas presented here are small and can be manufactured at a very low cost. The modified L-slot antenna can be integrated to compact communication devices. The sidewall ground and L-shape make this antenna conformal to right angle corners of the device casing. If the casing is metallic, it may serve as the ground plane and the sidewalls.

References

[1] T. Dissanayake and K. P. Esselle, "Correlation based pattern stability analysis and a figure of merit for UWB antennas," *IEEE Trans. Antennas Propag.*, vol. 52, no. 11, pp. 3184–3191, Nov. 2006.

[2] T. Dissanayakea, K. P. Esselle, and Y. Ge, "Integrated compact ultra-wideband L-shaped wide slot antennas," in *Proc. Asia-Pacific Microwave Conf.*, Dec. 4–7, 2005, vol. 1, pp. 16–18.

[3] M. Kahrizi, T. K. Sarkar, and Z. A. Maricevic, "Analysis of a wide radiating slot in the groundplane of a microstrip line," *IEEE Trans. Antennas Propag.*, vol. 41, no. 1, pp. 29–37, Jan. 1993.

[4] H.-L. Lee, H.-J. Lee, J.-G. Yook, and H.-K. Park, "Broadband planar antenna having a round corner rectangular wide slot," in *Proc. IEEE Int. Symp. on Antenna and Propagation*, Jun. 2002, vol. 2, pp. 460–463.

[5] P. Li, J. Liang, and X. Chen, "Ultra-wideband elliptical slot antenna fed by tapered microstrip line with U-shaped tuning stub," *Microw. Opt. Technol. Lett.*, vol. 47, no. 2, pp. 140–143, Oct. 2005.

[6] Y. F. Liu, K. L. Lau, Q. Xue, and C. H. Chan, "Experimental studies of printed wide-slot antenna for wide-band applications," *IEEE Antennas Wireless Propag. Lett.*, vol. 3, pp. 273–275, 2004.

[7] G. Sorbello, F. Consoli, and S. Barbarino, "Numerical and experimental study of a rectangular slot antenna for UWB communication," *Microw. Opt. Technol. Lett.*, vol. 44, no. 5, pp. 315–319, Mar. 2005.

[8] Y.-W. Jang, C.-C. Shin, and I.-M. Park, "Characteristics of ultraband printed slot antenna using FDTD method," *Microw. Opt. Technol. Lett.*, vol. 44, no. 2, Jan. 2005.

A Wideband Low-Profile Antenna Composed of a Conducting Body of Revolution and a Shorted Parasitic Ring

H. Nakano, H. Iwaoka, K. Morishita, and J. Yamauchi

***Abstract*—An antenna composed of a conducting body of revolution (BOR) and a parasitic ring shorted to a finite-sized ground plate, designated as the BOR-SPR, is designed for realizing a low-profile base station antenna with a wideband voltage standing wave ratio (VSWR) characteristic. The design of the BOR-SPR starts with a center-fed patch antenna. To match the antenna input impedance to a 50-ohm feed line, as a first step, a slot is cut into the patch (this antenna is designated as Ant-I), and as a second step, shorted parasitic conducting pins are added to the periphery of Ant-I (this antenna is designated as Ant-II). Ant-II has a VSWR bandwidth of approximately 28%. Further increase in the VSWR bandwidth is achieved by replacing the inner feed region of Ant-II with a conducting BOR. It is found that this replacement, creating the BOR-SPR, yields an extremely wide VSWR bandwidth of approximately 147%, where the electrical antenna height at the lower edge frequency of the bandwidth is small: approximately 0.07 wavelength. It is also found that the radiation pattern of the BOR-SPR is similar to that of a monopole above a finite-sized ground plate. The beam direction θ (measured from the direction normal to the surface of the BOR) varies between approximately 30° and 60°. The gain at $\theta = 60°$ is approximately 2 dBi near the lower edge frequency of the VSWR bandwidth and approximately 8 dBi near the upper edge frequency.**

***Index Terms*—Body of revolution (BOR), finite-difference time-domain (FDTD) analysis, shorted ring, wideband antenna.**

I. Introduction

Numerous multiband and wideband antennas have been developed [1]–[14] in response to the recent demand for wireless communication systems; for instance, the antenna in [10] is for dual-band operation around 2.4 and 5.2 GHz, while the antenna in [13] is for wideband operation ranging from 2.1–10.6 GHz (frequency band for UWB systems). These antennas are made of a thin-film and can be installed inside IT mobile devices, such as laptop computers and portable telephones.

The radiation element in each of the antennas in [6] and [12] stands upright above a conducting plate (ground plate), while maintaining the required frequency bandwidth of the VSWR. These antennas are used as base station antennas. One challenge in the design of such base station antennas is the reduction of the antenna height above the ground plate.

In general, if the antenna height is reduced, the bandwidth decreases. To overcome this decrease in bandwidth, so far, trials using a top-loading technique have been performed [4], [9]. The antennas in [4] and [9], where a patch is used for the top-loading element, show a bandwidth of approximately 15% and 138% for a $\mathrm{VSWR} = 1.93$ criterion (a -10 dB return loss criterion), respectively. Note that the antenna height in [9] is small: approximately $\mathrm{H} = 0.085\lambda_{\mathrm{low}}$, where λ_{low} is the operating wavelength at the lower edge frequency of the VSWR bandwidth.

This paper presents a novel wireless base-station wideband antenna with a low-profile structure. This antenna is composed of a conducting *b*ody *o*f *r*evolution (BOR) and a *s*horted *p*arasitic *r*ing, as shown in

Manuscript received January 12, 2007; revised September 14, 2007.

The authors are with the College of Engineering, Hosei University, Koganei, Tokyo 184-8584, Japan (e-mail: nakano@k.hosei.ac.jp).

Color versions of one or more of the figures in this paper are available online at http://ieeexplore.ieee.org.

Digital Object Identifier 10.1109/TAP.2008.917010

Fig. 1(d), and designated as the BOR-SPR antenna. The BOR-SPR originates from a center-fed low-profile patch antenna [referred to as the original patch antenna; see Fig. 1(a)] and reaches its final structure through two intermediate antenna structures (Ant-I and Ant-II).

The design process of the BOR-SPR is described in Section IV, which comprises the main part of this paper and starts with the analysis of the original patch. This original patch antenna is modified by cutting a ring slot into the patch [see the antenna in Fig. 1(b) designated as Ant-I] and then adding conducting pins shorted to the ground plate [see the antenna in Fig. 1(c) designated as Ant-II]. Ant-II exhibits a wideband VSWR characteristic (approximately 28% VSWR bandwidth).

The latter part of Section IV (i.e., Section IV-B) is an extension of the former part (i.e., Section IV-A). Section IV.B discusses how to further increase the VSWR bandwidth. For this purpose, the central patch (called the patch island) in Ant-II is replaced with a conducting BOR. The antenna based on the BOR [see Fig. 1(d)] is designated as the BOR-SPR antenna.

Optimization of the configuration of the BOR-SPR realizes a VSWR bandwidth of approximately 147% for a $\mathrm{VSWR} = 1.93$ criterion. The radiation pattern and gain within this VSWR bandwidth are also presented and discussed. Note that the antenna height H of the optimized BOR-SPR is electrically small: $\mathrm{H} = 0.071\lambda_{\mathrm{low}}$ at the lower edge frequency of the VSWR bandwidth. This height is approximately 16.5% smaller than the antenna height shown in [9].

II. Configuration

Fig. 1 shows the steps involved in reaching the final BOR-SPR antenna of Fig. 1(d) from the center-fed patch antenna of Fig. 1(a). The patch of diameter $\mathrm{D_{patch}}$ in Fig. 1(a), called the original patch, is excited through a vertical narrow strip line of width $\mathrm{W_{cent}}$, which is connected to the inner conductor of a coaxial feed line at the coordinate origin. In the second step, this original patch is transformed into a structure shown in Fig. 1(b), where a circular slot of width $\mathrm{W_{slot}}$ is cut in the original patch, yielding two sections: a small inner section (patch island of diameter $2\mathrm{x_1}$) and the remaining outer section (parasitic ring specified by inner diameter $\mathrm{D_{in,ring}}$ and outer diameter $\mathrm{D_{out,ring}} = \mathrm{D_{patch}}$). In the third step, the parasitic ring in Fig. 1(b) is shorted to the ground plate through $\mathrm{N_{pin}}$ conducting pins, each having width $\mathrm{W_{pin}}$, as shown in Fig. 1(c). In the fourth step, the central patch in Fig. 1(c) is replaced with a conducting BOR of diameter $2\mathrm{x_1}$, as shown in Fig. 1(d).

Except where noted, the following configuration parameters are used: $\mathrm{D_{GP}} = 136.7\ \mathrm{mm} \equiv \mathrm{D_{GP0}}$ for the ground plate (GP) diameter, $\mathrm{D_{patch}} = 40\ \mathrm{mm}\ (= \mathrm{D_{out,ring}})$ for the original patch diameter, $\mathrm{D_{in,ring}} = 20\ \mathrm{mm} \equiv \mathrm{D_{in,ring0}}$ for the inner diameter of the parasitic ring, $\mathrm{H} = 10$ mm for the antenna height above the ground plate, $2\mathrm{x_1} = 6.7$ mm for the diameters of the inner patch and the BOR, $\mathrm{W_{cent}} = 1.7$ mm for the strip line width, and $\mathrm{W_{pin}} = 1.4$ mm for the pin width (see Table I).

III. Analysis Method

The structures shown in Fig. 1(a) and (b) are symmetric with respect to both the x-z and y-z planes. If the number of shorting pins $\mathrm{N_{pin}}$ is even, then the structures in Fig. 1(c) and (d) are also symmetric with respect to both the x-z and y-z planes. For the following analysis we use the finite-difference time-domain method (FDTDM) based on Yee's mesh $\Delta\mathrm{x} \times \Delta\mathrm{y} \times \Delta\mathrm{z}$ [15]. For reducing the computation time, we use a subspace of $(\mathrm{x} \geq 0, \mathrm{y} \geq 0)$, that is, one-fourth of the total analysis space, taking advantage of both the x-z plane symmetry and the y-z plane symmetry.

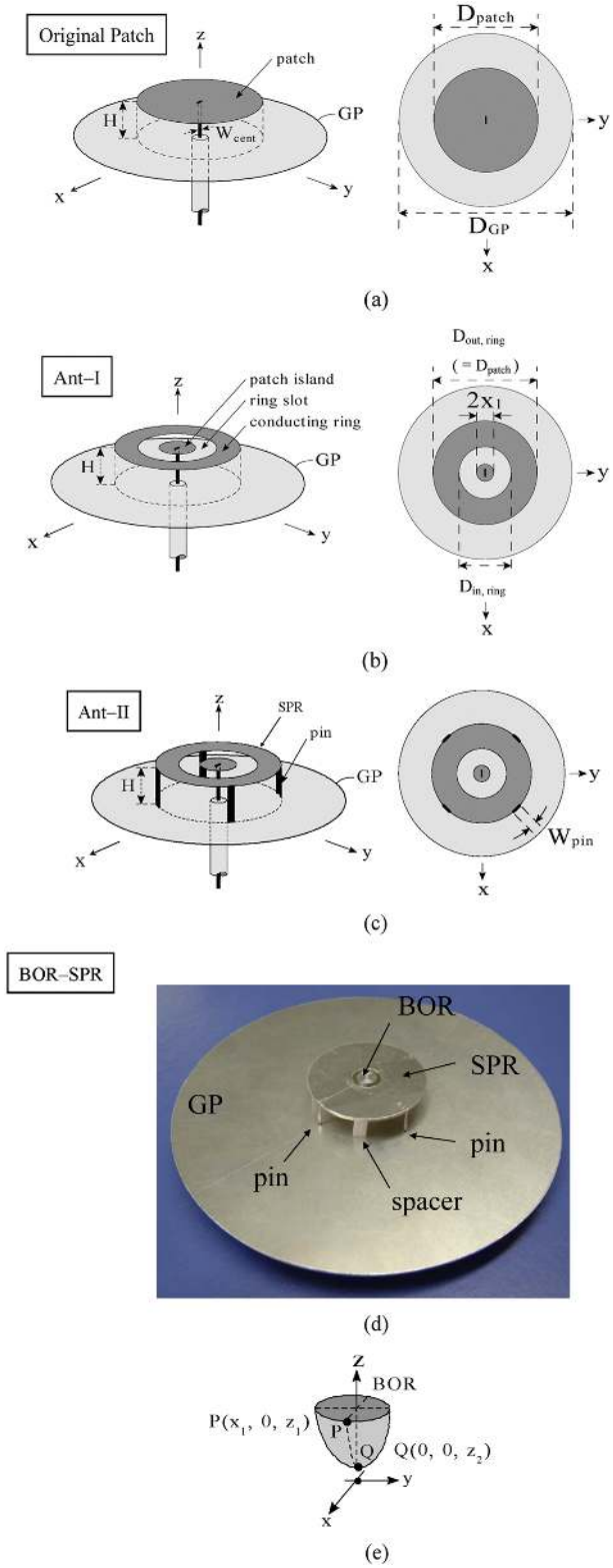

Fig. 1. Design process. (a) A center-fed low-profile patch antenna (original patch antenna). (b) Ant-I, where a ring slot is cut into the original patch. (c) Ant-II, where conducting pins are attached to Ant-I. (d) BOR-SPR, where the BOR is surrounded by a shorted parasitic ring. (e) Body of revolution (BOR).

The curved sections of the antenna structures in Fig. 1 are approximated using a stair function, for which the mesh size is chosen to be small relative to the wavelength: $\Delta\mathrm{x} = \Delta\mathrm{y} = \Delta\mathrm{z} = \lambda_{3.6}/200$, where $\lambda_{3.6}$ is the wavelength at a frequency of 3.6 GHz. In this case the ground

TABLE I
CONFIGURATION PARAMETERS USED FOR THE STRUCTURES SHOWN IN FIG. 1

symbol	value	unit
D_{GP0}	136.7	mm
$D_{out,\ ring}$	40	mm
H	10	mm
$2x_1$	6.7	mm
W_{pin}	1.4	mm
N_{pin}	4	——
z_1	10	mm
z_2	0.8	mm
x_0	1	mm

plane diameter $D_{GP0} = 328\Delta x (\approx 136.7$ mm). The FDTDM results for the selected mesh sizes are confirmed by the experimental results presented in Section IV.

The electric and magnetic fields in the entire antenna analysis space are used for calculating the antenna characteristics, including the input impedance, radiation pattern, and gain. For the radiation pattern calculation, the equivalence theorem [16] based on the electric current density $\mathbf{J}$ and magnetic current density $\mathbf{M}$ is employed, where the $\mathbf{E}$ and $\mathbf{H}$ fields surrounding the antenna are used for obtaining $\mathbf{J}(= \hat{n} \times \mathbf{H})$ and $\mathbf{M}(= \mathbf{E} \times \hat{n})$, for which $\hat{n}$ is the outward normal vector.

IV. DISCUSSION

A. Transformation From Original Patch to Ant-II

The mechanism of operation for the antenna shown in Fig. 1(a) is explained using an equivalent R-L-C circuit; the equivalent circuit takes into account the top-loaded monopole resonance due to the patch and feed pin [1], [4]. When a slot exists, as shown in the antennas of Fig. 1(b), (c), and (d), these antennas equivalently have two circuits: the first circuit expressing the region inside the slot and the second circuit expressing the region outside the slot. These two circuits are coupled electromagnetically. As seen later from Fig. 4, the first circuit for Fig. 1(d) is responsible for the radiation characteristics at high frequencies, and the VSWR bandwidth originally obtained by this first circuit is increased with the addition of the second circuit (due to parasitic effects).

The design of the antennas shown in Fig. 1 makes use of several electromagnetic concepts. The design starts with an investigation of the input impedance for the original patch shown in Fig. 1(a). The FDTDM analysis using frequencies around 3.75 GHz shows that the original patch has a large input reactance X_{in}, as seen in Fig. 2(a), i.e., the input impedance ($Z_{in} = R_{in} + jX_{in}$) does not match a 50-ohm feed line. This large reactance must be reduced to match the feed line.

The input reactance X_{in} is inductive and hence capacitance must be added to reduce the value of the inductance. This is achieved by cutting a ring slot into the original patch, as shown in Fig. 1(b); the slot equivalently forms capacitance. The structure in Fig. 1(b) is designated as Ant-I. Fig. 2(b) shows the input impedance of Ant-I. Compared with the original patch, Ant-I has lower reactance values around 3.75 GHz. However, an issue still exists in that the input resistance R_{in} is less than that required for 50-ohm impedance matching.

Generally, as the conducting volume of the antenna is decreased (and hence the conducting surface area is decreased), the antenna input resistance becomes smaller. Therefore, we can solve the issue of the low input resistance by increasing the conducting volume of Ant-I. This is done by adding conducting pins to the periphery of Ant-I, as shown in Fig. 1(c). This structure is designated as Ant-II.

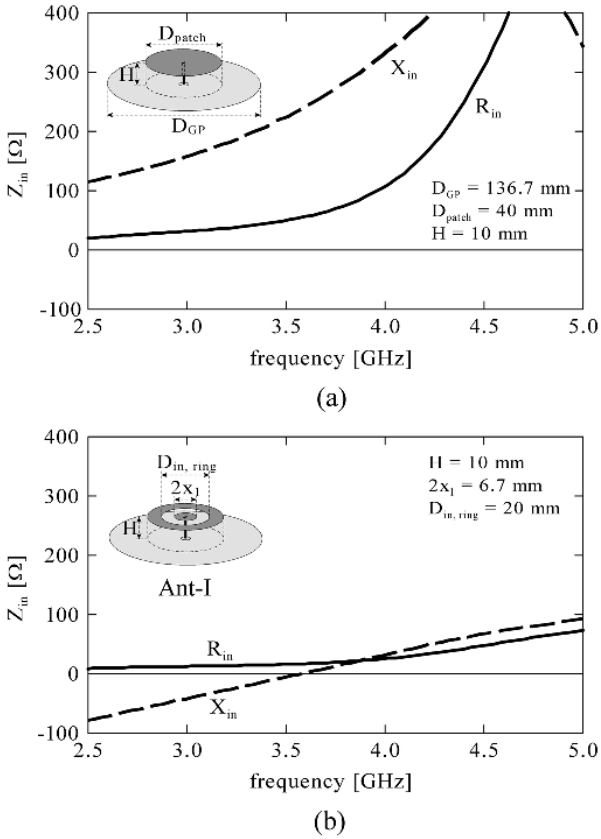

Fig. 2. Input impedances of (a) the original patch and (b) Ant-I for $D_{in,\ ring} = 20$ mm $\equiv D_{in,\ ring0}$. Note that the original patch and Ant-I have the same ground plate diameter $D_{GP} = 136.7$ mm $\equiv D_{GP0}$.

We vary the number of conducting pins N_{pin} from 0 to 8. Note that these pins are shorted to the ground plate, and the spacing between neighboring pins is $2\pi/N_{pin}$ [rad]. It is found that an optimum value for the number of pins to realize a wideband VSWR characteristic is found to be $N_{pin} = 4$. In this case, a bandwidth of approximately 28%, ranging from $f_L = 3.12$ GHz to $f_H = 4.13$ GHz, for a $VSWR = 1.93$ criterion (a -10 dB return loss criterion) is obtained. For the following analysis the number of pins is fixed to be $N_{pin} = 4$.

B. Modification of Ant-II; Replacement of the Patch Island With a Conducting Body of Revolution

The central section of Ant-II [Fig. 1(c)] is a patch island of diameter $2x_1$ connected to a vertical feed strip of width W_{cent}. We replace this central section with a conducting body of revolution (BOR) whose diameter at the top surface is $2x_1$, as shown in Fig. 1(d). This modified structure of Ant-II is designated as the BOR-SPR antenna (BOR surrounded by a *s*horted *p*arasitic conducting *r*ing). Note that the small spacer supporting the antenna is foam polystyrene whose relative permittivity is close to 1.

The BOR is illustrated in detail in Fig. 1(e), where the edge point P and bottom point Q are specified with coordinates $(x, y, z) = (x_1, 0, z_1)$ and $(x, y, z) = (0, 0, z_2)$, respectively. The generating line of the BOR is defined by an exponential function of $x = -x_0 \exp[-t(z - z_1)] + x_0 + x_1$, where x_0 is an arbitrary constant and t is a constant given by $t = [\log(1 + x_1/x_0)]/[z_1 - z_2]$. The constant x_0 is chosen to be the same value as that used for widening the VSWR bandwidth of a card-type fan-shaped UWB antenna in [13] ($x_0 = 1$ mm), where the value x_0 is obtained through iteration.

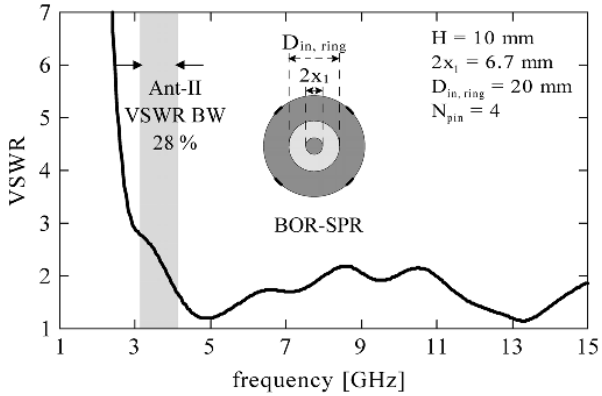

Fig. 3. VSWR of BOR-SPR for $D_{in,\,ring} = 20\ \text{mm} = D_{in,\,ringo}$ and $D_{GP} = 136.7\ \text{mm} = D_{GP0}$.

The width of the slot (spacing) between the BOR and the shorted parasitic ring is given as $W_{slot} = (D_{in,\,ring} - 2x_1)/2$. Table I shows the BOR-SPR configuration parameters that are fixed for the following analysis. Only the inner ring diameter $D_{in,\,ring}$ (and hence, W_{slot}) is varied subject to the objectives of the analysis.

Fig. 3 shows the VSWR of the BOR-SPR, where the inner ring diameter is $D_{in,ring} = 20\ \text{mm} \equiv D_{in,\,ringo}$ used for Ant-II. As seen from this figure, the BOR-SPR can be easily matched to a 50-ohm transmission line above 4 GHz. However, the VSWR below 4 GHz is high. In the following analysis, we try to improve the VSWR below 4 GHz by varying the inner ring diameter $D_{in,\,ring}$. The variation in $D_{in,\,ring}$ corresponds to varying the capacitance between the BOR and shorted parasitic ring.

Fig. 4(a)–(c) shows the frequency response of the VSWR for three values of $D_{in,\,ring}$. Note that Fig. 4(c) shows the limiting case, where the spacing between the BOR and the shorted parasitic ring is zero $(D_{in,\,ring} = 2x_1)$, and hence the top surface is a simple plane. Fig. 4(a)–(c) shows that the lower edge frequency of the bandwidth can be moved downward by appropriately choosing $D_{in,\,ring}$ (i.e., the spacing between the BOR and the shorted parasitic ring). The lower edge frequency for $D_{in,\,ring} = 10$ mm is improved to approximately 2 GHz (the analysis is confirmed by the experimental results; see the white dots). Consequently, the bandwidth for a $\text{VSWR} = 1.93$ criterion is expanded to approximately 147% (a frequency range of 2.15–14 GHz). Note that the upper edge frequency of the VSWR bandwidth is not sensitive to changes in the inner ring diameter $D_{in,\,ring}$.

It is worth considering how an isolated BOR without a shorted parasitic ring behaves. Fig. 4(d) presents the VSWR characteristic of the BOR used for the BOR-SPR in this section. A comparison of Fig. 4(d) with Fig. 4(a) and (b) shows that the shorted parasitic ring is a key factor in obtaining the wideband VSWR characteristic of the BOR-SPR.

The representative theoretical radiation pattern as a function of frequency is shown in column B in the middle of Fig. 5, where the inner ring diameter is chosen to be the value that results in an approximately 147% VSWR bandwidth (i.e., $D_{in,\,ring} = 10$ mm, using the configuration parameters shown in Table I. The radiation patterns in columns A and C are explained later, where the same $D_{in,\,ring} = 10$ mm but different D_{GP} are used). It is found that the BOR-SPR behaves like a monopole above a finite-sized ground plate. It is also found that the beam direction deviates from the z-axis and varies between approximately $\theta = 30^\circ$ and 60°, where θ is an angle measured from the z-axis. In addition, as the frequency decreases, the level of the cross-polarization component in the horizontal plane [x-y plane, see Fig. 5(b)] decreases.

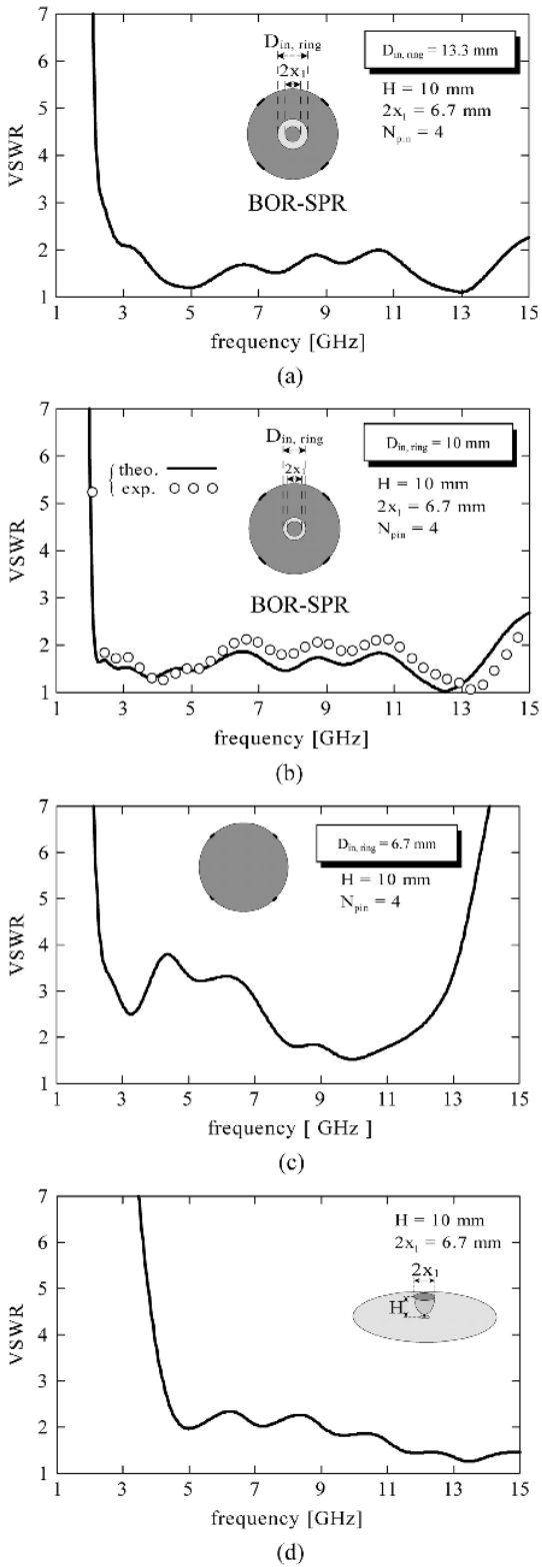

Fig. 4. VSWR characteristics of BOR-SPR. The inner ring diameter is (a) $D_{in,\,ring} = 13.3$ mm, (b) $D_{in,\,ring} = 10$ mm, and (c) $D_{in,\,ring} = 6.7\ \text{mm} = 2x_1$. (d) VSWR characteristic of an isolated BOR. All the structures in Fig. 4 have the same ground plate diameter $D_{GP} = 136.7\ \text{mm} = D_{GP0}$.

The absolute gain for $D_{in,\,ring} = 10$ mm and $D_{GP} = 136.7\ \text{mm} \equiv D_{GP0}$ is shown by the solid line in Fig. 6, where the gain is observed in a fixed direction of $\theta = 60^\circ$. The experimental results are also presented using white dots. The gain of the VSWR bandwidth is approximately

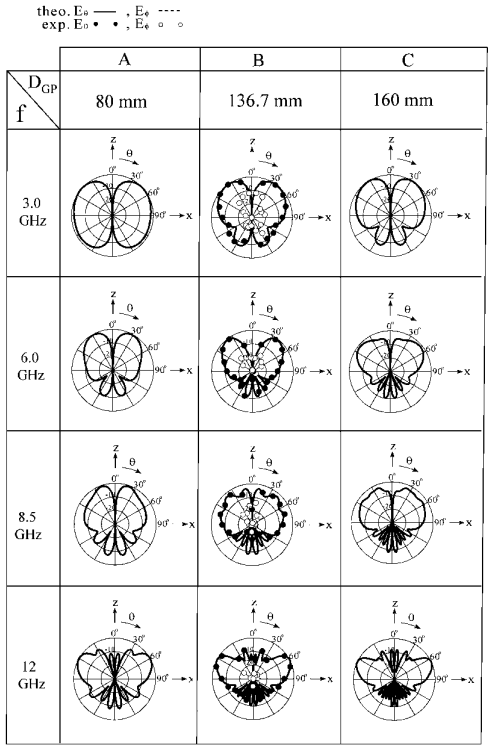

(a)

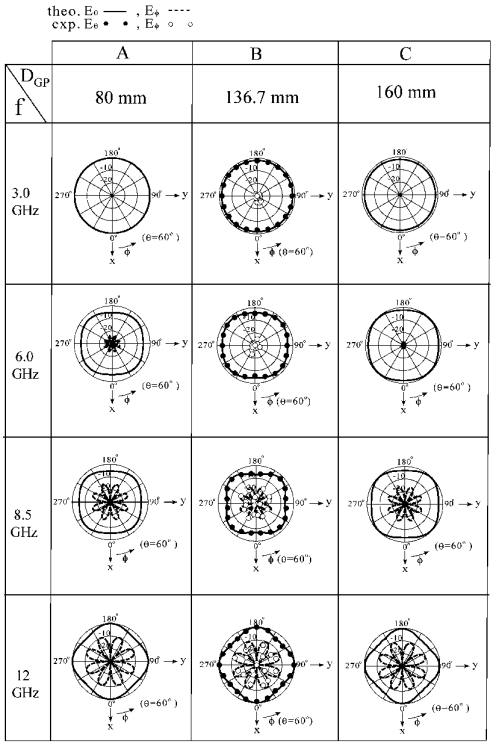

(b)

Fig. 5. Radiation pattern of BOR-SPR for $D_{in,\ ring} = 10$ mm. The diameter of the ground plate is $D_{GP} = 80\ \text{mm} < D_{GP0}$ in column A, $D_{GP} = 136.7\ \text{mm} = D_{GP0}$ in column B, and $D_{GP} = 160\ \text{mm} > D_{GP0}$ in column C.

2 dBi near the lower edge frequency and approximately 8 dBi near the upper edge frequency. The smallest gain at approximately $f = 8.5$ GHz results from the fact that the radiation in the $\theta = 60^\circ$ direction exhibits a minimum (valley) in the ripple of the radiation pattern.

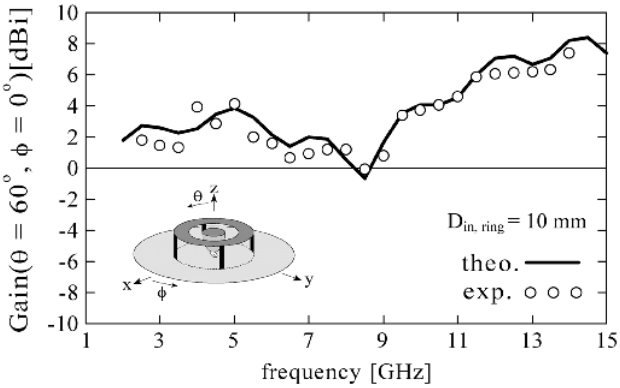

Fig. 6. Gain in the $\theta = 60^\circ$ direction of BOR-SPR for $D_{in,\ ring} = 10$ mm and $D_{GP} = 136.7\ \text{mm} = D_{GP0}$.

We briefly explain the experimental work here. The VSWR shown in Fig. 4(b) was obtained using a network analyzer (HP-8510 C). The experimental radiation patterns shown in column B of Fig. 5 were obtained using a wideband antenna (ETS double-ridged guide antenna). The experimental gain in Fig. 6 (white dots) is obtained by comparing the gains of six reference horn antennas; each antenna is responsible for part of the frequency range from 1–18 GHz (1.00–2.60 GHz, 2.60–3.95 GHz, 3.95–5.85 GHz, 5.40–8.20 GHz, 8.20–12.40 GHz, and 12.40–18.00 GHz).

So far, the ground plane diameter has been kept constant at $D_{GP} = 136.7\ \text{mm} \equiv D_{GP0}$. This is based on the fact that there is little change in the input impedance when D_{GP} is greater than D_{GP0}. Further analysis is preformed to reveal the effect on the radiation pattern of having a finite ground plate. Columns A and C of Fig. 5 show the radiation patterns for $D_{GP} = 80\ \text{mm} < D_{GP0}$ and $D_{GP} = 160\ \text{mm} > D_{GP0}$, in comparison with the radiation pattern for $D_{GP} = D_{GP0}$. It is found that the effect of the ground plane diameter on the radiation pattern in the x-z plane is noticeable at low frequencies. Note that the maximum radiation intensity for $D_{GP} = \infty$ is always found in the $\theta = 90^\circ$ direction (horizontal plane) for the analysis frequency range of 1 and 15 GHz (not illustrated in Fig. 5).

Lastly, we compare the BOR-SPR with a top-loaded patch antenna called *Set 2* in [9]. The frequency bandwidths (BWs) using a $\text{VSWR} = 1.93$ criterion (a -10 dB return loss criterion) for these two antennas are given, together with the antenna height H; $(\text{BW},\ \text{H}) = (147\%, 10\ \text{mm}) = (147\%, 0.071\lambda_{\text{low}})$ for the BOR-SPR and $(\text{BW},\ \text{H}) = (138\%, 34\ \text{mm}) = (138\%, 0.085\lambda_{\text{low}})$ for the antenna Set 2, where the antenna height H is normalized to the wavelength (λ_{low}) at the lower edge frequency of the VSWR bandwidth for each antenna. The VSWR bandwidth of the BOR-SPR is approximately $9\%[= 147\%–138\%]$ wider with a $16.5\%[= (0.085\lambda_{\text{low}} - 0.071\lambda_{\text{low}})/0.085\lambda_{\text{low}}]$ smaller antenna height. It can be said that the BOR-SPR realizes an antenna with a smaller height and a wider VSWR bandwidth, when compared with the antenna Set 2.

V. Conclusion

A design process for realizing a low-profile base station antenna composed of a conducting body of revolution (BOR) and a shorted parasitic conducting ring (SPR) is presented. The finite-difference time-domain method (FDTDM) is used in the analysis. The computation time for the FDTDM is reduced using the symmetry of the antenna structure; the basic calculation for the FDTDM is done in one-fourth of the total computation space.

First, a low-profile center-fed round patch of diameter D_{patch} above a ground plate, designated as the original patch, is transformed into

a new antenna, designated as Ant-I, by cutting a ring slot into the patch; the slot divides the original patch into a patch island (of diameter $2x_1$) and a parasitic ring (inner diameter $D_{in,\ ring}$ and outer diameter $D_{out,\ ring} = D_{patch}$). Analysis is performed over a frequency range of 2.5–5.0 GHz. It is found that the slot is effective in reducing the high input reactance of the original patch X_{in} around 3.75 GHz. However, the input impedance of Ant-I is not suitable for impedance matching to a 50-ohm feed line, due to the small input resistance R_{in}.

To increase the input resistance R_{in}, an extended version of Ant-I, designated as Ant-II, is investigated. In Ant-II, the parasitic ring is shorted to the ground plate through conducting pins. It is revealed that the input impedance of Ant-II can be matched to a 50-ohm feed line if the number of conducting pins N_{pin} is appropriately chosen. An Ant-II with $N_{pin} = 4$ has a frequency bandwidth of 28% for a $VSWR = 1.93$ criterion (a -10 dB return loss criterion).

Further increase in the VSWR frequency bandwidth is achieved by replacing the patch island with a conducting body of revolution (BOR). The generating line of the BOR is defined by an exponential function. The antenna is designated as the BOR-SPR. Analysis of the BOR-SPR shows a wider VSWR bandwidth than Ant-II, with a lower edge frequency of approximately 4 GHz.

Finally, the lower edge frequency of the VSWR bandwidth is decreased by varying only the inner ring diameter $D_{in,\ ring}$ (corresponding to varying the width of the slot). It is found that, as $D_{in,\ ring}$ is decreased ($D_{in,\ ring}$ approaches $2x_1$), the lower edge frequency decreases. Consequently, a wide VSWR bandwidth of approximately 147% is realized.

In addition to the VSWR investigation, the radiation pattern and gain for the BOR-SPR having an approximately 147% VSWR bandwidth are theoretically obtained and confirmed with experimental results. It is found that the radiation pattern exhibits a monopole-like pattern, where the beam direction (BD) deviates from the direction normal to the top surface of the BOR, due to the finite size of the ground plate; the BD varies between approximately $\theta = 30^\circ$ and 60°. The gain observed in the $\theta = 60^\circ$ direction is approximately 2 dBi near the lower edge frequency of the VSWR bandwidth and approximately 8 dBi near the upper edge frequency.

ACKNOWLEDGMENT

The authors thank V. Shkawrytko for his assistance in the preparation of this manuscript.

REFERENCES

[1] C. Delaveaud, P. Leveque, and B. Jecko, "New kind of microstrip antenna: The monopolar wire-patch antenna," *Electron. Lett.*, vol. 30, no. 1, pp. 1–2, 1994.

[2] H. Nakano, N. Ikeda, Y. Wu, Y. Suzuki, H. Mimaki, and J. Yamauchi, "Realization of dual-frequency and wide-band VSWR performances using normal-mode helical and inverted-F antennas," *IEEE Trans. Antennas Propag.*, vol. 46, no. 6, pp. 788–729, Jun. 1998.

[3] H. Nakano, M. Fukasawa, and J. Yamauchi, "Discrete multiloop, modified multiloop, and plate-loop antennas—Multifrequency and wide-band VSWR characteristics," *IEEE Trans. Antennas Propag.*, vol. 50, no. 3, pp. 371–378, Mar. 2002.

[4] J. S. Row, S. H. Yeh, and K. L. Wong, "A wide-band monopole plate-patch antenna," *IEEE Trans. Antennas Propag.*, vol. 50, no. 9, pp. 1328–1330, Sep. 2002.

[5] J. Kraus and R. Marhefka, *Antennas*, 3rd ed. New York: McGraw-Hill, 2002, ch. 8.

[6] T. Taniguchi and T. Kobayashi, "An omnidirectional and low-VSWR antenna for the FCC-approved UWB frequency band," in *Proc. IEEE Antennas and Propagation Society Int. Symp.*, Jun. 2003, vol. 3, pp. 460–463.

[7] S. Y. Suh, W. L. Stutzman, and W. A. Davis, "A new ultrawideband printed monopole antenna: The planar inverted cone antenna (PICA)," *IEEE Trans. Antennas Propag.*, vol. 52, no. 5, pp. 1361–1364, May 2004.

[8] C. Balanis, *Antenna Theory*, 3rd ed. New York: Wiley, 2005, ch. 11.

[9] K.-L. Lau, P. Li, and K.-M. Luk, "A monopole patch antenna with very wide impedance bandwidth," *IEEE Trans. Antennas Propag.*, vol. 53, no. 2, pp. 655–661, Feb. 2005.

[10] H. Nakano, Y. Sato, H. Mimaki, and J. Yamauchi, "An inverted FL antenna for dual-frequency operation," *IEEE Trans. Antennas Propag.*, vol. 53, no. 8, pt. 1, pp. 2417–2421, Aug. 2005.

[11] H. Nakano, H. Iwaoka, H. Mimaki, and J. Yamauchi, "A wideband PSP antenna radiating a linearly polarized conical beam," in *Proc. 18th Int. Conf. on Applied Electromagnetics and Communications*, Dubrovnik, Croatia, Oct. 2005, pp. 541–544.

[12] K. Morishita, J. Yamauchi, and H. Nakano, "A standing-type fan-shaped broadband antenna—Part 2," in *Proc. IEICE (Institute of Electronics, Information and Communication Engineers) General Conf.*, Tokyo, Japan, Mar. 24–27, 2006, B-1-164.

[13] H. Nakano, T. Kondo, and J. Yamauchi, "A card-type, fan-shaped antenna for wide band operation," *Int. J. Microw. Opt. Technol.*, vol. 1, no. 1, pp. 100–105, Jun. 2006.

[14] H. Nakano, "Recent progress in broadband antennas," in *ISAP*, Singapore, Nov. 2006, [CDROM] a367 r66.

[15] K. S. Yee, "Numerical solution of initial boundary value problems involving Maxwell's equations in isotropic media," *IEEE Trans. Antennas Propag.*, vol. AP-14, pp. 302–307, May 1966.

[16] R. F. Harrington, *Time-Harmonic Electromagnetic Fields*. New York: McGraw-Hill, 1961, pp. 106–110.

Dielectric and Conductor Loss Quantification for Microstrip Reflectarray: Simulations and Measurements

Harish Rajagopalan and Yahya Rahmat-Samii

***Abstract*—The conductor and dielectric loss mechanisms in microstrip reflectarray are described using simulation models and waveguide measurements. The dielectric constant and loss tangent variation with frequency is obtained for a particular substrate using existing datasheets. Variable size patch reflectarray element was studied for loss characterization. The effect of these losses is characterized and the potential cause for the loss phenomenon is provided. It is observed that the dielectric loss and copper loss occur near the patch resonance due to strong electric fields in the substrate region below the patch and the large currents on the top surface of the patch, respectively.**

***Index Terms*—Conductor loss, dielectric loss, reflectarray.**

I. INTRODUCTION

Microstrip reflectarrays present an alternative to the conventional parabolic reflectors [1], [2]. The reflectarray consists of individual radiating elements printed on a grounded substrate. A plane wavefront can be obtained by controlling the scattering properties of each element. A feed is used to illuminate the reflectarray surface. The basic design

Manuscript received July 2, 2007; revised September 26, 2007. This work was supported in part by the Jet Propulsion Laboratory, California Institute of Technology, under a contract with the National Aeronautics and Space Administration.

The authors are with the Department of Electrical Engineering, University of California, Los Angeles, Los Angeles, CA 90095 USA (e-mail: harish@ee.ucla.edu; rahmat@ee.ucla.edu).

Color versions of one or more of the figures in this paper are available online at http://ieeexplore.ieee.org.

Digital Object Identifier 10.1109/TAP.2008.919225